Baghdad Science Journal

Volume 23 | Issue 1 Article 1

1-1-2026

Structural Design of Macroporous Layered Double Hydroxide Catalysts: Alleviating Mass Transport Constraints in Bulkier Triglycerides

Nazrizawati Ahmad Tajuddin
School of Chemistry and Environmental, Faculty of Applied Sciences, Universiti Teknologi MARA, 40450 Shah Alam, Selangor, Malaysia, nazriza@uitm.edu.my

Mohamad Hidayat Haider
Chemical Engineering Department, Faculty of Science and Technology, Universitas Jambi, 36361, Jambi, Indonesia, hidayathaider@uitm.edu.my

Nazarudin Nazarudin
Chemical Engineering Department, Faculty of Science and Technology, Universitas Jambi, 36361, Jambi, Indonesia, nazarudin@unja.ac.id

How to Cite this Article

Tajuddin, Nazrizawati Ahmad; Haider, Mohamad Hidayat; and Nazarudin, Nazarudin (2026) "Structural Design of Macroporous Layered Double Hydroxide Catalysts: Alleviating Mass Transport Constraints in Bulkier Triglycerides," *Baghdad Science Journal*: Vol. 23: Iss. 1, Article 1.
DOI: https://doi.org/10.21123/2411-7986.5133

BAGHDAD SCIENCE JOURNAL 2026;23(1):1–15

SPECIAL ISSUE ARTICLE

Structural Design of Macroporous Layered Double Hydroxide Catalysts: Alleviating Mass Transport Constraints in Bulkier Triglycerides

Nazrizawati Ahmad Tajuddin [1,*], **Mohamad Hidayat Haider** [2], **Nazarudin Nazarudin** [2]

[1] School of Chemistry and Environmental, Faculty of Applied Sciences, Universiti Teknologi MARA, 40450 Shah Alam, Selangor, Malaysia
[2] Chemical Engineering Department, Faculty of Science and Technology, Universitas Jambi, 36361, Jambi, Indonesia

ABSTRACT

Layered double hydroxides (LDHs) serve as potential catalysts for biodiesel production through triglyceride (TAG) transesterification; nevertheless, mass transport limitations hinder their effectiveness, especially with larger TAG molecules. This study addresses this limitation by synthesizing macroporous MgAlLDH and ZnAlLDH using a polystyrene templating method. Thorough characterization reveals the successful formation of macroporous structures with significantly increased physicochemical properties and their structural design compared to conventional LDHs. X-ray Diffraction (XRD) confirmed the successful restoration of the LDH structure following calcination and rehydration, with enhanced crystallinity seen in the macroporous materials. The BET surface area analysis revealed a substantial increase (~10x for MgAlLDH) in the macroporous framework. Scanning Electron Microscopy (SEM) and Transmission Electron Microscopy (TEM) images revealed a macroporous network with an average pore diameter of ~300 nm, consistent with the dimensions of the polystyrene template. The X-ray Photoelectron Spectroscopy (XPS) analysis revealed slight changes in surface elemental composition and oxidation states, indicating the impact of the macroporous structure on surface properties. Catalytic testing with various TAGs (C4–C18) demonstrates a notable enhancement in catalytic activity, particularly for higher TAGs, due to improved mass transfer. The turnover frequencies of macroporous materials significantly exceed those of conventional LDHs, exceeding them by approximately 20 times for the MgAlLDH system and 15 times for the ZnAlLDH system. The findings highlight the efficacy of macroporous LDHs as very effective catalysts for biodiesel production, overcoming the inherent mass transfer limitations of conventional LDH catalysts.

Keywords: Biodiesel, Layered Double Hydroxides (LDH), Macroporous, Mass transfer, Triglycerides

Introduction

The worldwide transition to renewable energy and sustainable practices has elevated the need for alternative fuels, especially biodiesel. Biodiesel, produced by the transesterification of triglycerides (TAGs), is a sustainable and environmentally friendly alternative to traditional fossil fuels.[1] Nonetheless, its manufacture encounters considerable obstacles, especially with catalyst efficiency. Layered double hydroxides (LDHs) have arisen as potential catalysts due to their distinctive structural and chemical characteristics.[2,3] Conventional LDHs face mass transport limitations, particularly when dealing with larger TAG molecules, despite their promising applications. Thus, this work investigates the design and synthesis of macroporous MgAl and ZnAl layered double hydroxides (LDHs) via a polystyrene templating technique to overcome these limitations. The use of macropores in catalysts aims to enhance mass transfer and improve catalytic performance, especially for larger TAGs. The results

Received 20 February 2025; revised 23 May 2025; accepted 3 June 2025.
Available online 1 January 2026

* Corresponding author.
E-mail addresses: nazriza@uitm.edu.my (N. A. Tajuddin), hidayathaider@uitm.edu.my (M. H. Haider), nazarudin@unja.ac.id (N. Nazarudin).

International Conference on Discoveries in Applied Sciences and Applied Technology (DASAT2025)
https://doi.org/10.21123/2411-7986.5133

offer guidance on surmounting the intrinsic constraints of LDH-based catalysts, facilitating enhanced and scalable biodiesel synthesis.

The effectiveness of transesterification processes in biodiesel generation is greatly affected by the molecular size of TAGs and the properties of the catalysts used. A larger number of TAG molecules frequently experience steric hindrances, resulting in decreased conversion rates. In our previous study,[4] we have explored these difficulties and providing insights into possible remedies. The study found that hydrothermally activated ZnAlLDH exhibited superior performance in the transesterification of triglycerides (C4 to C18) with methanol, compared to those activated via cold liquid phase or vapor phase reconstruction.[4] In some manner, the transesterification of longer-chain triacylglycerols (C8 to C18) required the addition of 20 wt. % 1-butanol to improve solubility and an increase in reaction temperature to 110 ˚C to achieve comparable conversion rates. Similarly, another study[5] noted that the catalytic efficacy of the reconstituted NiAlLDHs was assessed in the transesterification of model triglycerides (C4 to C12) with methanol to provide fatty acid methyl esters (FAMEs), a crucial constituent of biodiesel. The findings indicated that the NiAlLDHs had significant catalytic activity, with the Ni: Al ratio being pivotal in influencing the efficacy of the transesterification process. Somehow, it was hindered by steric and mass transport limitations, particularly for bulkier TAG molecules (e.g., C12). These larger molecules struggled to access the active catalytic sites due to restricted pore sizes and the intrinsic layered structure of the catalysts. Elevated reaction temperatures (e.g., 110 ˚C) were required to partially overcome these barriers, but the overall conversion efficiency remained lower compared to smaller TAGs (e.g., C4). Both results underscore the importance of structural modifications, such as introducing macropores, to enhance mass transfer and improve catalytic performance for larger TAGs.

This paper describes a unique method for enhancing biodiesel production by synthesizing macroporous MgAl and ZnAl layered double hydroxides (LDHs) with a polystyrene template, as can be seen in Fig. 1. Unlike normal LDHs, which have mass transport restrictions when converting bulky triglycerides (TAGs), the added macroporosity improves reactant diffusion and access to active sites. This structural alteration, together with optimized M^{2+}/M^{3+} metal ratios, results in enhanced catalytic performance, especially for long-chain TAGs (C12 to C18), without the need for high temperatures or solvent additions. This study provides a physically and functionally improved catalyst design for more efficient and scalable biodiesel synthesis by directly addressing the steric and diffusion obstacles encountered in previous investigations.

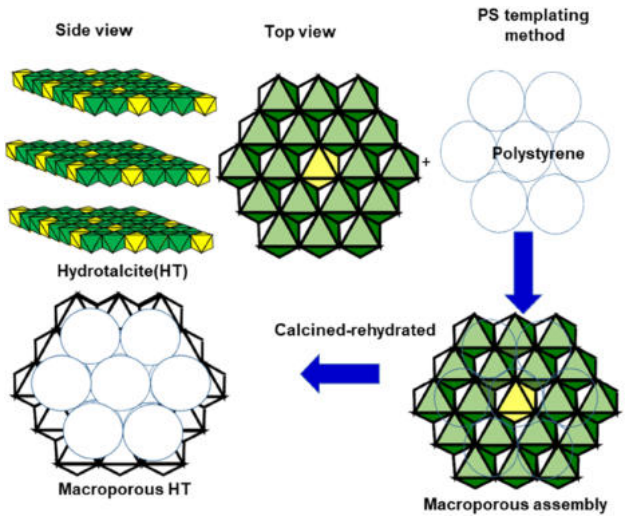

Fig. 1. The schematic layered double hydroxide macroporous templating view incorporating polystyrene beads.

Materials and methods

Catalyst preparation

All reagents used were of analytical quality and required no additional purification, and all catalytic synthesis ingredients were procured from Merck and Sigma-Aldrich. The triglycerides (TAGs) ranging from C4 to C18 were acquired from Alfa Aesar. This methodology follows the approach described in our previous work.[5] Polystyrene beads were made through an emulsion polymerization process without an emulsifier. At 80 ˚C, 20 ml of distilled water was used to dissolve potassium persulfate (0.35 g). A round-bottom flask was filled with water (1500 ml) and subjected to nitrogen purging throughout the night. To remove polymerization inhibitors, 140 ml of styrene and 27 ml of divinylbenzene were rinsed with a 0.1 M sodium hydroxide solution (in a 1:1 ratio) and thoroughly washed with distilled water. The washing step was repeated twice, followed by the addition of the styrene-divinylbenzene mixture and a dropwise addition of a potassium persulfate solution. After stirring, the mixture was left overnight. This allows sufficient time for the polymerization reaction, initiated by potassium persulfate, to proceed to completion. Extended reaction time ensures proper cross-linking and integration of the styrene-divinylbenzene network onto or within the substrate, promoting uniform material formation and optimal structural properties. The material was

filtered, washed with ethanol and deionized water, then dried at 70 ˚C for 8 hours.

The preparation of standard alkali-free LDHs (ConvMgAlLDH and ConvZnAlLDH, in a 4:1 ratio) was carried out through co-precipitation of 1.5 M magnesium nitrate hexahydrate, 1.5 M zinc nitrate hexahydrate, and 1.5 M aluminium nitrate nonahydrate using a 500 ml Radleys flask system. During synthesis, the pH was carefully maintained at 8.5 for ConvMgAlLDH[6] and 9.5 for ConvZnAlLDH.[7] The mixture was then subjected to an aging process at 65 ˚C overnight. To activate the catalysts, ConvMgAlLDH and ConvZnAlLDH (also referred to as the CAL sample) underwent calcination. The as-synthesized (AS) catalysts were heated at 450 ˚C under an oxygen flow and at 300 ˚C for five hours, respectively. The calcination temperature is customized according to the thermal stability and decomposition characteristics of each layered double hydroxide (LDH) system, with thermal behavior varying by metal cation. MgAl-LDH generally decomposes at elevated temperatures (~400–500˚C) due to the enhanced thermal stability of Mg-based hydroxides. ZnAl-LDH, conversely, often commences decomposition at a lower temperature (~300–400˚C), due to the weaker M–OH interactions in Zn-based LDHs, which may provide various oxide phases following thermal exposure. Prior to the calcination procedure, a Thermal Gravimetric Analysis (TGA) was conducted, revealing thermal temperatures of 450 ˚C and 300 ˚C for the ConvMgAlLDH and ConvZnAlLDH catalysts, respectively. Following calcination, the hydrothermal method (HTM) was applied to rehydrate the catalyst. This process involved stirring the calcined sample in water until it was evenly dispersed, then transferring it to a hydrothermal flask and heating it at 110–150 ˚C. The material was centrifuged, rinsed with deionized water, and dried at 80 ˚C for 8 hours.

Building upon the methodologies outlined by Geraud et al.,[8] macroporous LDH (MacroMgAlLDH and MacroZnAlLDH) was synthesized through a modified version of the approach introduced by Woodford et al.[9] This work marks the first successful synthesis of alkali-free MacroMgAlLDH and MacroZnAlLDH. For the synthesis, 1 M solutions of Mg^{2+}, Zn^{2+}, and Al^{3+} salts were prepared using 100 ml of deionized water to establish the required 4:1 ratio. A separate solution of 2 M ammonium nitrate was prepared in deionized water (100 ml), serving as the precipitating agent without the addition of alkali. Polystyrene beads (6 g) were suspended in an equal ratio of ethanol and water in a four-neck round-bottom flask and stirred continuously at 65 ˚C. The M^{2+}:Al^{3+} solution and ammonium carbonate were introduced dropwise at a controlled rate of 1 ml/min using an automated pump. To maintain the desired pH, ammonium hydroxide was gradually added, following the established procedure. After aging overnight at 65 ˚C, the resulting material was filtered and washed with deionized water until the pH reached 7. The final product underwent calcination and subsequent rehydration, following the standard LDH preparation protocol.

Catalyst characterization

X-ray powder diffraction (XRD) measurements were conducted using a PANalytical X'pert Pro instrument (model DY 2536), operating at 45 kV and 40 mA. Scans were conducted across a 2θ range of 10 ˚ to 80˚, and crystallite sizes were estimated using the Scherrer equation. X-ray photoelectron spectroscopy (XPS) analysis was performed using a Kratos Axis HSi spectrometer, equipped with monochromated Al Kα radiation at 90 W. The system featured a charge neutralization unit and a magnetic focusing lens. Data processing and spectral deconvolution were performed using CasaXPS software (v2.3.16), with the C 1s peak (284.5 eV) serving as an internal binding energy reference. For nitrogen porosimetry, a Quantachrome Autosorb iQ2 analyzer was used after the samples were degassed at 120 ˚C for three hours. Surface area calculations were based on the desorption branch of the isotherm at relative pressures (P/P_0) below 0.2, following the Brunauer, Emmett, and Teller (BET) approach. Base site densities were measured by CO_2 pulse titration using a Quantachrome ChemBET 3000 chemisorption system with a thermal conductivity detector.[10] Prior to titration, a 50 mg sample was transferred into a quartz cell, treated under helium flow at 120 ˚C for one hour, then cooled to 40 ˚C before successive 50 l CO_2 pulses were introduced at ambient temperature until adsorption saturation was reached.

Thermogravimetric analysis (TGA) coupled with online mass spectrometry (MS) was conducted using a SETARAM thermal analyzer under nitrogen flow, with the temperature ramped up to 800 ˚C at a heating rate of 10 ˚C/min. Scanning electron microscopy (SEM) images were captured using a JEOL JSM-7000F system at 20 kV with a detector for energy-dispersive X-ray spectroscopy (EDS). Transmission electron microscopy (TEM) was conducted at 200 kV using a JEOL 2100F FEG STEM microscope. Samples were initially dispersed in methanol and deposited onto perforated carbon-coated copper grids before imaging.

Biodiesel reaction

The transesterification of triglycerides (C4-C18) was carried out using LDH catalysts in a Radley's Starfish reactor. A reaction mixture containing 10 mmol of tributyrin (2.93 cm^3), 308 mmol of methanol (12.5 ml), and 0.0025 mol of dihexyl ether (0.59 cm^3) was prepared in a three-necked flask. At the initial time point (t = 0), 0.15 cm^3 of collected specimen were analyzed using Gas Chromatography-Flame Ionization Detection (GC-FID).[11] Subsequently, the catalyst (50 mg) was introduced into the system, and the reaction was conducted under continuous stirring at 65 ˚C and 650 rpm for 24 hours. To evaluate triglyceride (TAG) conversion and fatty acid methyl ester (FAME) formation, aliquots were extracted, filtered, and dissolved in 1.6 cm^3 of dichloromethane (DCM) before being transferred into gas chromatography vials. Analysis was performed using a Shimadzu GC-2010 Plus system (Japan), fitted with a Zb-50 capillary column (30 m × 0.32 × mm × 0.25 μm) and an autosampler.[12] The GC oven temperature was programmed to begin at 60˚C (held for 1minute), then ramped at 10˚C/min to 220˚C, with a final hold of 10minutes. Under this temperature-programmed method, retention times for FAMEs ranged from approximately 3 to 19minutes, depending on their carbon chain length and degree of unsaturation. Retention time varies because each compound possesses a distinct combination of boiling point, molecular size, and unsaturation, which influences its interaction with the stationary phase. To ensure the accuracy and reliability of the data, all reactions were performed in triplicate. The chromatographic results provided insights into conversion rates, product outputs, initial reaction kinetics, and turnover frequency (TOF). The initial reaction kinetics were determined based on the linear segment of the conversion response curve within the initial 60 minutes. FAME selectivity was calculated using the equation:

$$\frac{[FAME]}{[MAG] + [DAG] + [FAME] + [GLY]} x\ 100 \quad (1)$$

where

[FAME] is Fatty acid methyl ester,
[MAG] is a monoacylglyceride,
[DAG] is a diacylglyceride and
[GLY] is glycerol.

Results and discussion

The X-ray diffraction (XRD) patterns confirmed the successful synthesis of the layered double hydroxides (LDHs), as illustrated in Fig. 2. The diffraction patterns for ConvMgAlLDH and MacroMgAlLDH in Fig. 2a and Fig. 2b correspond closely to the characteristic hydrotalcite structure, consistent with previous reports in the literature.[13] The observed diffraction peaks of as-synthesized (AS) at $2\theta = 11.6^\circ$, 23.4˚, 35.0˚, 39.6˚, 47.1˚, 61.1˚, and 62.3˚ are indicative of MgAlLDH, confirming the formation of the desired material.[8,9] These peaks match the JCPDS card number 22–0700, further validating the LDH structure.[13,14] Notably, a slight elevation in intensity around $2\theta = 20^\circ$ in the MacroMgAlLDH (AS) sample in Fig. 2b suggests the presence of residual amorphous polystyrene template within the structure, which is yet to be removed by thermal treatment.

Upon calcination at 450 ˚C on both ConvMgAlLDH and MacroMgAlLDH samples, the characteristic brucite-like layers collapsed, leading to a phase transformation into MgO (periclase), as confirmed through the emergence of distinct peaks recorded at $2\theta = 35.9^\circ$, 43.5˚, and 63.5˚, corresponding to the (111), (200), and (220) planes, respectively.[15] These peaks align with the JCPDS card number 45-0946 for MgO[16] as illustrated in Fig. 2a and Fig. 2b, CAL. The disappearance of basal reflections of d(003) and d(006) further confirmed the structural collapse of the LDH framework during the calcination process.[11] Following rehydration, the reappearance of diffraction peaks corresponding to basal planes d(003), d(006), d(009), d(015), d(018), d(110), d(113), and d(116) confirmed the effective reconstruction of the LDH framework as shown in Fig. 2a and Fig. 2b, HTM.[17,18] This restoration process validated the reversible nature of the *Memory Effect* LDH structure upon rehydration, consistent with hydrotalcite-like materials (JCPDS 22–0700).

The reconstructed LDH's purity is evaluated by calculating the relative intensity of HT peak d(003) to the mixed oxide peak d(012) through the formula: [$_y$HT/ ($_y$HT + $_y$mixed oxide)] x 100 %, where $_y$ represents the intensity difference (y_2–y_1).[11] The HTM reconstruction has enhanced the ConvMgAlLDH and MacroMgAlLDH crystallinity from 75.9% (AS) to 81.2% (HTM) and from 83.3% to 85.3%, respectively. The incorporation of PS templates and the subsequent reconstruction led to an increase in the lattice parameters *a* and *c* of the MacroMgAl LDH,[11] indicating a larger crystallite size, as can be seen in Table 1.

The effective synthesis of both ConvZnAlLDH and MacroZnAlLDH was confirmed and illustrated in Fig. 2c and Fig. 2d, respectively. The AS samples exhibiting distinct basal reflections at d(003), d(006),d(012), d(015), d(018), d(0111), and d(110) align with the hydrotalcite structure and correspond to JCPDS card 38−0487.[17] An amorphous peak detected at approximately $2\theta = 20^\circ$ indicates the

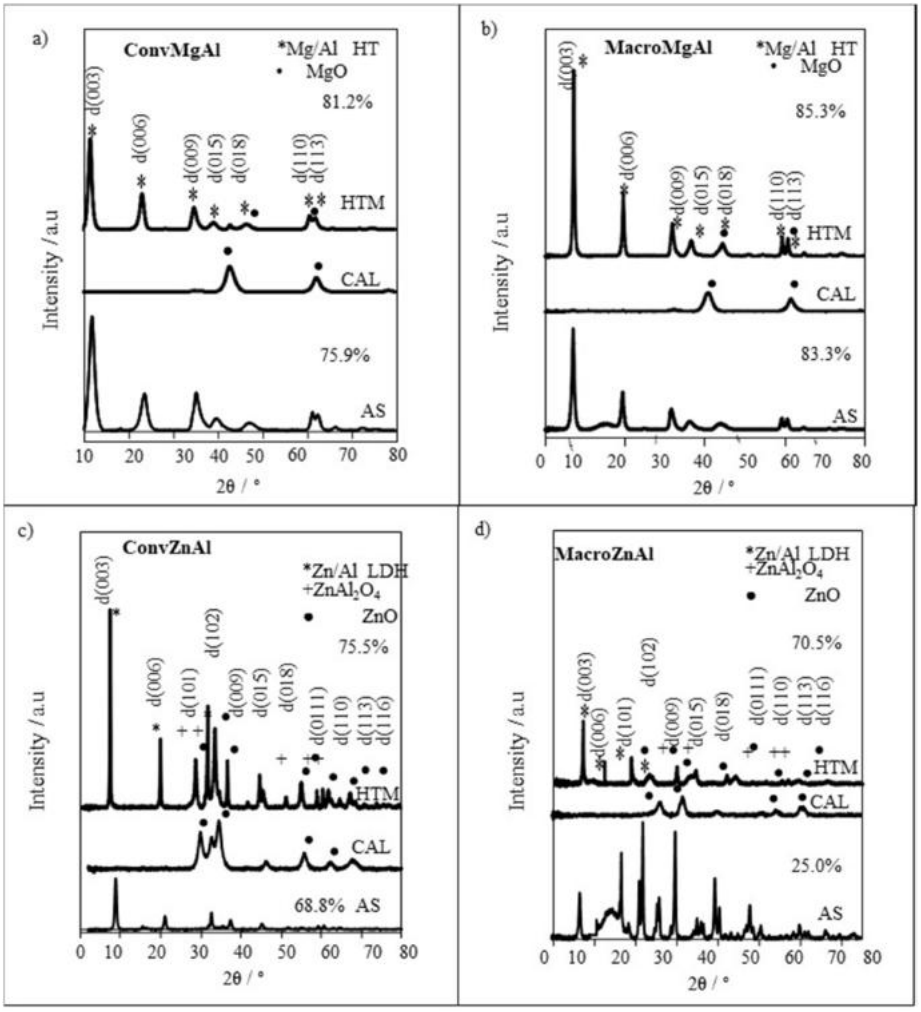

Fig. 2. XRD analysis involving standard and upgraded MgAl-LDH and ZnAl-LDH, showing their crystalline structures.

presence of a polymer template, which was partially preserved in the structure. Calcination at 350 ˚C induced a complete phase transition, characterised by the vanishing of LDH peaks and the introduction of new reflections associated with ZnO (JCPDS 36−1451) and $ZnAl_2O_4$ (JCPDS 05−0669) phases. The prominent peaks for ZnO are seen at $2\theta = 31.8^{\circ}$, 34.5˚, and 36.3˚, whereas those for $ZnAl_2O_4$ are found at $2\theta = 31.2^{\circ}$, 44.5˚, and 59.1˚, therefore substantiating the thermal decomposition of the LDH and the synthesis of mixed oxides. The rehydration of the calcined ConvZnAlLDH and MacroZnAlLDH effectively reinstated the LDH structure, as seen by the reemergence of basal reflections d(003), d(006), and d(009), signifying the restoration of interlayer water and structural integrity. An increase in crystallinity was observed upon reconstruction, rising from 68.8% (AS) to 75.5% (HTM) in ConvZnAlLDH. For MacroZnAlLDH, the increase was from 25% (AS) to 70.5% (HTM). A reduction was observed in both crystallite size and the lattice parameters a and *c* as a result of the MacroZnAlLDH form. This is explained by the possibility of ZnO and $ZnAl_2O_4$ forming and penetrating the interlayers, which would have a detrimental effect on the layer's reformation, reduce the lattice parameter, and also decrease the crystallite size, as shown in Table 1.

Fig. 3a-b depicts the N_2 adsorption-desorption isotherms for both the standard and macroporous variants of MgAlLDH and ZnAlLDH, respectively. The ConvLDH isotherms are categorized as type II with H2 hysteresis loops as referring to IUPAC classification,[19] signifying that the catalysts comprise mesopores with an 'ink-bottle' morphology.[20] The restricted pore accessibility in ConvLDH, compared to MacroLDH, is due to its confined channel-like morphology.[11]

The MacroMgAlLDH and MacroZnAlLDH both exhibit isotherms characteristic of multilayer adsorption and capillary condensation, featuring type II and IV isotherms with H3 hysteresis loops that

Table 1. Comparison of textural parameters for standard and high-porosity MgAl-LDH and ZnAl-LDH, detailing basal spacing d(003), lattice constant, and crystallite sizes.

		[a]Lattice constant /nm		
Parameter/ catalyst	d003 / nm	*a*	*c*	[b]Crystallite size / nm
MgAlLDH				
ConvMgAlLDH	0.74	0.304	2.28	13.5
MacroMgAlLDH	0.74	0.305	2.29	23.2
ZnAlLDH				
ConvZnAlLDH	0.74	0.308	2.28	36
MacroZnAlLDH	0.74	0.306	2.28	19.1

*[a] Determined through the Bragg equation, whereas [b] was estimated using the Scherrer equation.

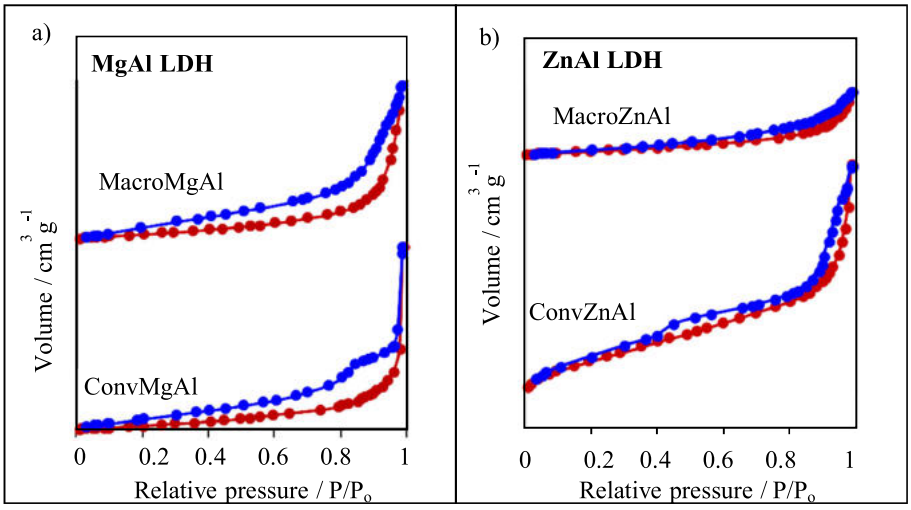

Fig. 3. Overlay of sorption isotherms for (a) standard and high-porosity MgAl-LDH and (b) ZnAl-LDH.

indicate the formation of integrated mesopore-macropore complexes.[11] The presence of slit-shaped pores is also indicated, arising from the plate-like morphology.[21] A mercury infiltration test was performed to better analyze and study the pore network. ConvMgAlLDH and ConvZnAlLDH have mesoporous pore sizes (31 and 25 nm, respectively), also known as interparticulate spacings, as can be seen in Fig. 4a-b. In agreement with previous researches,[21,22] MacroLDH variants of these two formulations produce macroporous voids immediately, measuring 106 nm and 146 nm, respectively. This is supported by the use of PS templates, which enhance the distance between hydrotalcite clusters and therefore considerably enhance the availability of the basic catalyst. A concentration of 100 to 200 nm has been reported in several prior research utilizing mercury intrusion porosimeters to quantify the pore network distribution of hydrotalcite.[22] Except for the MacroMgAlLDH material, which has a slightly larger range, the pore size distribution profiles of the two materials exhibit a single-mode pore diameter, as seen by a tight distribution across all samples. For the first time, this study demonstrates the effective synthesis of macroporous hydrotalcite.

The effectiveness of PS beads was verified, and their size distribution was measured using SEM imaging, as shown in Fig. 5a. The image confirmed that the beads had a fully spherical shape, and the average diameter of the beads was found to be 375 nm. SEM images of both catalysts were obtained to initially examine the differences in morphology between conventional and macroporous LDH; these are shown in Fig. 5b. ConvMgAl exhibits the classic morphology of sand roses. ConvZnAl materials have a greater surface area (~100 nm), which may be explained by the hexagonal platelets exhibiting plate-plate overlap observed in this material. In both MgAl and ZnAl, the macropore network is readily seen within the MacroHT structure. The macropores in MacroMgAl HT and MacroZnAl HT have typical widths of 316 nm and 270 nm. These numbers are marginally less than the PS bead templates' measured diameter, most likely as a result of the beads' shrinkage during

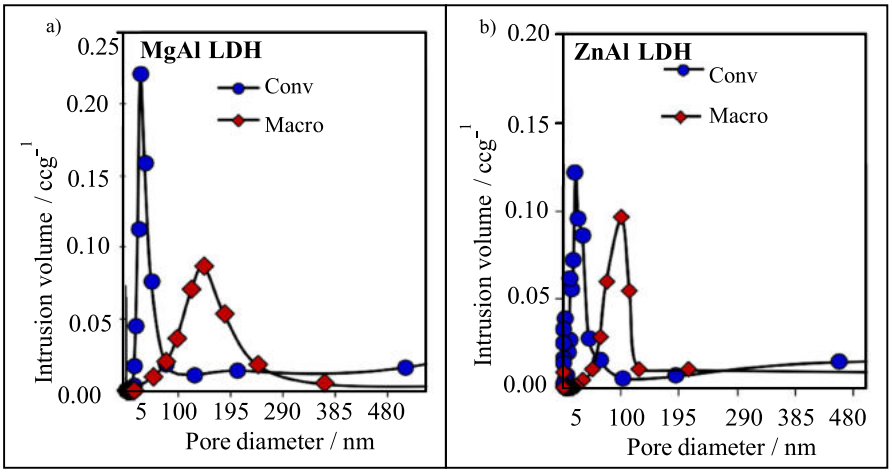

Fig. 4. Comparison of pore size distributions for standard and high-porosity of MgAl-LDH (left) and ZnAl-LDH (right), based on porosity analysis.

the calcination process. In accordance with the pore distributions determined by the mercury intrusion porosimeter, these findings also show that macropores have been successfully incorporated into the hydrotalcite framework. First, the PS beads are eliminated by calcination, exposing the structure's obvious voids. Owing to the materials' *Memory Effect*, XRD has demonstrated that rehydration has restored the layer. When the PS template was removed following the calcination-rehydration process, organized thin-walled macropores were revealed by an HR-STEM analysis of the MacroMgAl and MacroZnAl shown in Fig. 5c. The PS range and SEM results were aligned with the average pore diameter of 300 nm. PS bead templated macropore networks frequently experience macropore shrinkage as a result of contraction that occurs in the calcination process. The findings align with a prior study[23] that found that MacroMgAlLDH had a mean pore width of 310 nm, which was derived based on a PS bead diameter of 350 nm. The materials were comparable since the nominal ratio in both MacroMgAl studies was 4:1. The heterogeneous macropore structure of MacroZnAlLDH suggested a less-than-ideal synthesis method for PS inclusion. At 250 nm, the macropore void was observed, which is somewhat smaller than the 270 nm SEM data. This problem could be resolved by changing the thermal processing approach to a dissolving strategy.

The DRIFTS spectra for the ConvLDH and MacroLDH series are shown in Fig. 5d, respectively. DRIFTS examination of typical hydrotalcite samples often shows three distinct zones. The surface OH stretching mode is shown by the first region between 3000 and 3800 cm^{-1}, which corresponds to the water absorbed in the hydrotalcite lamellar structure.[24,25] Another way to think of this is as a water molecule bending mode that happens at about 1600 cm^{-1}. The OH stretching vibration seen at 3700 cm^{-1} indicates that hydroxyl groups are present at the corners or edges of the MgO structure.[11] ConvLDH and MacroLDH of MgAl showed a wide peak at 3773 cm^{-1} and a distinct peak at 3711 cm^{-1}, respectively, in our investigation. This provides additional evidence that LDH is converted to MgO during calcination and that this process is reversed upon rehydration, as shown by XRD analysis. The substantial water stretching mode in this region indicates that rehydration has enhanced the volume of water integrated into the structures. This notion is further corroborated by the XRD, which indicates that the quantity of rehydrated material exceeds that of the precursor. In all samples, the C-O vibration happens at 2847 cm^{-1}. In the 1700–1300 cm^{-1} range, overlapping infrared bands were seen in every LDH series. CO_3^{2-} bonding, which mostly includes unidentate and bidentate bonding types, takes place between 1400 and 1665 cm^{-1}.[26] Magnesium bound to carbonates is visible at 1405 cm^{-1}. The identification of a Mg-O vibration in the 950–700 cm^{-1} range indicates the development of hydrotalcite.[11] Except a few bands that exhibit slight variations, ZnAlLDH typically exhibits infrared spectra that are comparable to those of MgAlLDH. Both ZnAl samples (ConvLDH and MacroLDH) showed a shoulder at about 3300 cm^{-1}, which is a sign of a weak hydroxyl group vibration. This shoulder coincides with the major OH vibration observed at 3700 cm^{-1}, further demonstrating OH bonding.[11,27] According to Montanari et al.,[28] octahedral Al ($Al_{VI}OH$) is recorded at 3733 cm^{-1}, while the major band happens at 3695 cm^{-1}.[11] On the other hand, tetrahedral Al connected to OH ($Al_{IV}OH$) is indicated by the peak observed at 3778

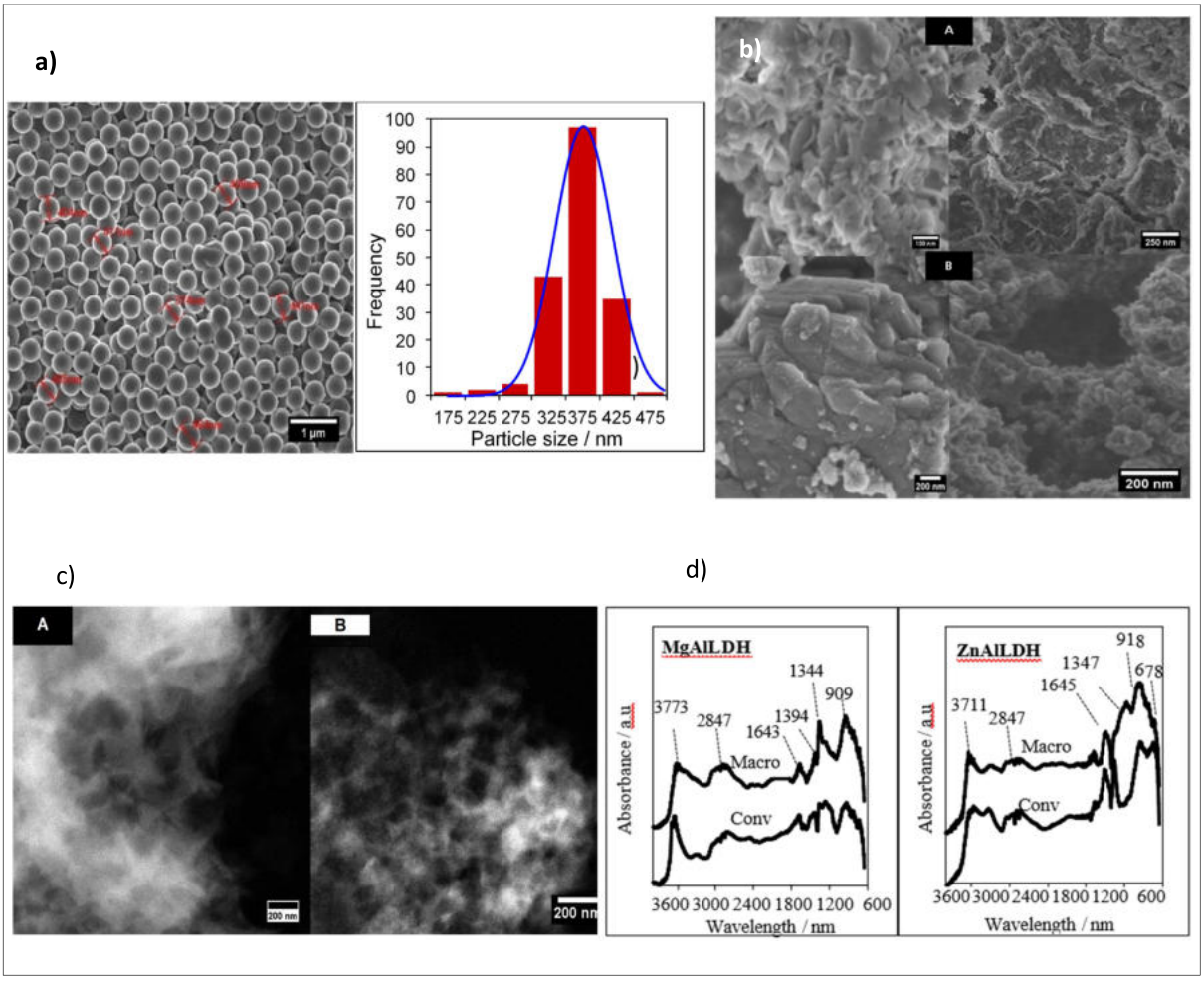

Fig. 5. (a) Morphological analysis of polystyrene spheres using SEM, accompanied by their particle size distribution. (b) Electron microscopy images of MgAl-LDH (A) and ZnAl-LDH (B), comparing standard (left) and high-porosity (right) structures. (c) High-resolution imaging of MacroMgAl-LDH (A) and MacroZnAl-LDH (B), highlighting their structural details. (d) Infrared analysis of ConvMgAl-LDH, ConvZnAl-LDH to be compared with MacroMgAlLDH and MacroZnAlLDH, highlighting differences between standard and high-porosity forms.

cm^{-1}. The tetrahedral and octahedral Al peaks may overlap at the same wavelength,[11] making it difficult to distinguish between them.

The TGA measurements indicate notable disparities between conventional and macroporous LDH, as listed in Table 2. For MgAlLDH, the macroporous structure exhibits a somewhat reduced water weight loss (11.47%) relative to the conventional sample (14.5%). However, it demonstrates a markedly increased carbonate weight loss (9.75% against 5.74%), resulting in comparable total weight loss for both structures. Conversely, the MacroZnAlDH sample demonstrates a greater water weight loss (17.26% vs. 12.11%) and a much lower carbonate weight loss (4.34% vs. 9.95%) relative to the conventional sample, leading to a slightly reduced overall weight loss (21.60% vs. 22.06%). The observed water loss in MacroZnAlLDH surpasses its predicted value, indicating improved water retention attributed to the macroporous architecture, but the reduced carbonate weight loss implies either a lower carbonate content or incomplete release. The observation verified that the MacroZnAlLDH sample contains a higher density of interlayer H_2O compared to the other three samples. The results demonstrate that the macroporous structure markedly affects the breakdown behavior of LDH, improving water retention in ZnAlLDH and amplifying carbonate release in MgAlLDH relative to conventional LDH. A general equation for HTs, $[M(II)_{1-x}M(III)_x(OH)_2]\chi^+(A^{n-}\chi/n)\ mH_2O$, was used to evaluate both theoretical and experimental weight loss, as well as the LDH composition.[11] This method has been used to determine the weight loss of all samples, both theoretically and experimentally, as can be found in Table 2. The total mass reduction observed in the experiment aligns well with the theoretical

Table 2. Comparison of theoretical and experimental weight loss based on the LDH formula determined from thermal and compositional analyses.

Measured Weight Loss (experimental) (%)				Calculated Weight Loss (theoretical) (%)			
LDH catalyst/ weight loss	H_2O exp	CO_3 exp	Total Weight loss/ %	H_2O theory	CO_3 theory	Total Weight loss / %	LDH formula
Conventional LDH							
MgAl	14.49	5.74	20.24	9.36	7.2	16.56	$[Mg_{0.77}Al_{0.23}(OH)_2].(CO_3)_{0.12}0.57H_2O$
ZnAl	12.11	9.95	22.06	10.44	7.2	17.64	$[Zn_{0.77}Al_{0.23}(OH)_2].(CO_3)_{0.12}0.58H_2O$
Macroporous LDH							
MgAl	11.47	9.75	21.22	9.36	9	18.36	$[Mg_{0.71}Al_{0.29}(OH)_2].(CO_3)_{0.15}0.52H_2O$
ZnAl	17.26	4.34	21.60	10.8	12.6	23.4	$[Zn_{0.59}Al_{0.41}(OH)_2].(CO_3)_{0.21}0.60H_2O$

Table 3. Elemental M^{2+}:Al^{3+} ratio obtained from compositional analysis of standard and high-porosity LDH.

	Conventional LDH		Macorporous LDH	
Nominal Metal to Aluminum Catalyst Ratio (M^{2+}: Al^{3+})	EDX	XPS	EDX	XPS
Mg:Al4:1	3.31	1.02	2.42	1.15
Zn:Al:4:1	3.33	2.28	1.45	1.02

prediction, despite the fact that these results slightly contradict those of a prior research.[23] To determine the true bulk and surface compositions, EDX and XPS were used to further analyze a range of conventional and macroporous MgAl and ZnAl LDH with a nominal ratio of 4, as shown in Table 3.[11] The macroporous samples exhibit a lower bulk M^{2+}:Al^{3+} ratio compared to their conventional LDH counterparts in both samples. When evaluating future reactivity differences, it is essential to differentiate enhancements driven by morphological or structural effects from those influenced by elemental composition or inherent basicity.[11,23]

The elemental composition of MgAl materials at the surface was subsequently examined using XPS. The spectra of Mg 2s, Al 2p, and O 1s are shown in Fig. 6a-c, respectively.[11] The spectra were calibrated at a binding energy of 284.6 eV using the C 1s peak from adventitious carbon. The strong interaction between metal atoms and the oxide is evident from the prominent peak at 90 eV[11] in the spectra shown in Fig. 6a. Two components were identified by deconvoluting the Al 2p spectra as shown in Fig. 6b: tetrahedral Al (Al-Mg) at 72.7 eV and octahedral Al (Al-O interaction) at 74.8 eV.[11] This observation is consistent with the Al-MAS NMR reporting that there was a slightly higher octahedral Al in MgAl HTM than tetrahedral Al. The O 1s spectra of the typical MgAl hole transport material (HTM) is shown in Fig. 6c. The parent state seen at 530 eV is consistent with previous research. Two separate components were found via peak deconvolution. The oxygen associated with carbon species (CO^{2-}) is shown by the large peak at 531 eV, whereas the O species in OH^- structures are represented by the less noticeable peak at 533 eV. As the Mg^{2+} content in MacroMgAlLDH increases, the O^{2-} intensity increases linearly. Later, the ZnAlLDH series' surface was examined using XPS. Fig. 6d-f shows the Zn 2p XP, Al 2p XP, and O 1s XP spectra, respectively.[11] Based on the NIST spectrum database,[29] the Zn 2p spectra in Fig. 6d were fitted at 1020 and 1042 eV, which correspond to the spin-orbit split Zn $2p_{3/2}$ and $2p_{1/2}$ states, respectively. The Al 2p spectra in Fig. 6e were shown at 74.5 eV and included two components that showed tetrahedral Al at 71.8 eV and octahedral Al at 74.0 eV.[11] At 532 eV, peak deconvolution showed two separate components in the O 1s spectra. O associated with carbon species (CO_3^{2-}) is shown by the conspicuous peak at 530 eV, whereas O species in OH^- structures are represented by the less significant peak at 533 eV. As demonstrated by CO_2-TPD in Fig. 7, the O^{2-} intensity decreased with macroporosity, suggesting a lower in the strength of basic sites corresponding to higher Zn content.[11] CO_2 binding on LDH can be classified into three regions: bicarbonate (weakly basic), bidentate carbonate (moderately basic), and unidentate (strongly basic). Both series exhibit a combination of medium basicity (300–450 °C) and strong basicity (above 450 °C).[11]

Table 4 shows that in MgAlLDH samples, the base site density reduced from 5.8×10^{-19} to 2.7×10^{-19}

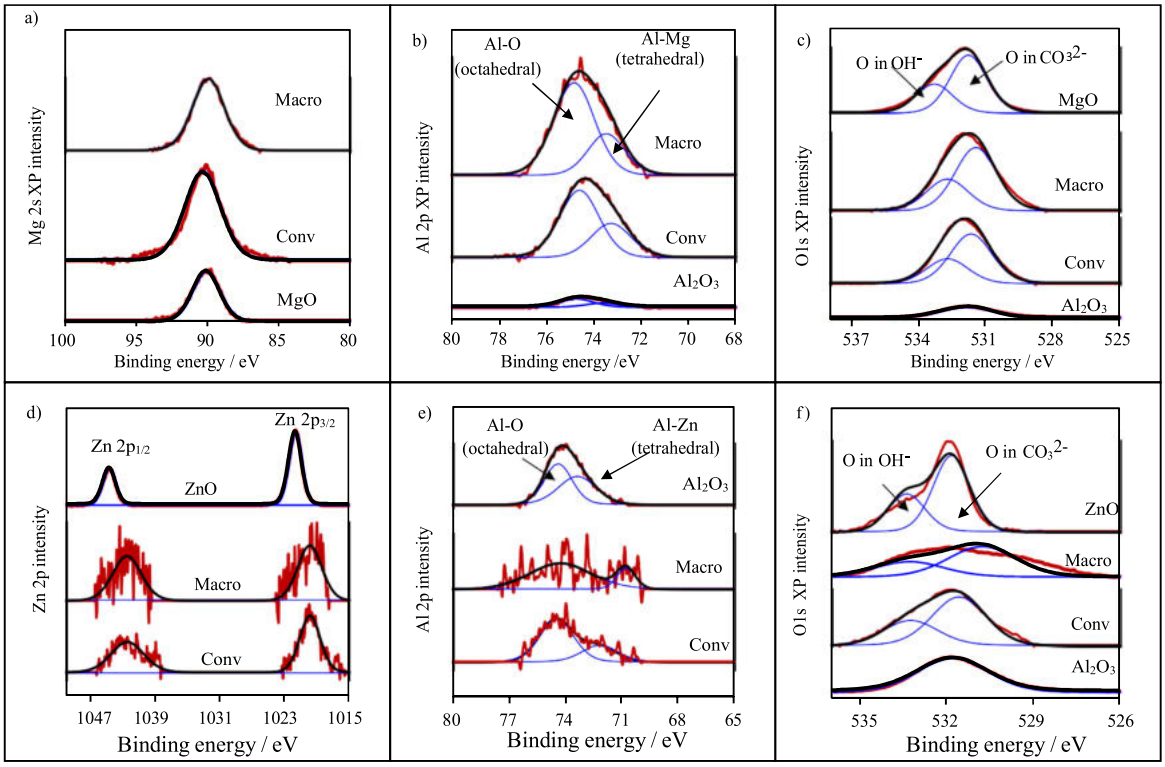

Fig. 6. ConvHT and MacroHT MgAl (a-c) and ConvHT and MacroHT ZnAl (d-f) displaying characteristic elemental signals.

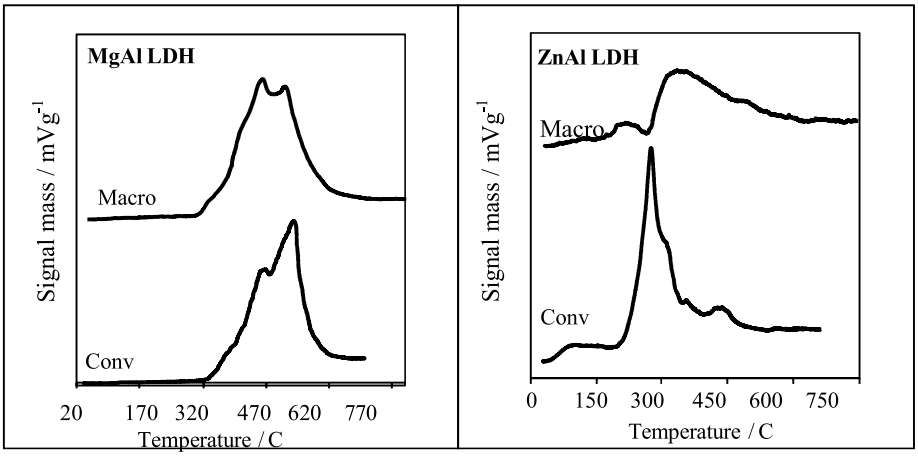

Fig. 7. CO_2-TPD analysis involving conv and macro-porosity MgAl-LDH and ZnAl-LDH.

molecules/g, while the active sites decreased from 0.057 mmol/g in ConvLDH to 0.045 mmol/g in MacroLDH. Likewise, with ZnAlLDH, the base site density decreased from 6.0×10^{-19} to 2.8×10^{-19} molecules/g, while the active sites decreased from 0.100 mmol/ g in ConvLDH to 0.046 mmol/g in MacroHT. The injection of acidic components from the polystyrene (PS) template, which lessens the basic character of MacroLDH samples, is probably the cause of this decrease in basicity with macroporosity. Following that, the bulk and surface compositions of a number of ConvLDH and MacroLDH of the MgAl and ZnAl series were examined using EDX and XPS, as shown in Table 3. The macroporous samples' bulk M^{2+}: Al^{3+} ratio is smaller than that of traditional LDH, which is essential for assessing reactivity changes. The materials' adsorption and catalytic qualities may be impacted by this variation in bulk ratio. This may be attributable to the acidic components from PS diminishing the basicity of MacroHT.[11]

To further evaluate the effectiveness of conventional and macroporous catalysts in producing FAME,

Table 4. Active number count and base site density determined from CO_2-TPD analysis.

Catalysts	Number of active sites (mmol/g)	Base site density (molecules/g) (10^{-19})
Conventional LDH		
MgAl	0.057	5.8
ZnAl	0.100	6.0
Macroporous LDH		
MgAl	0.045	2.7
ZnAl	0.046	2.8

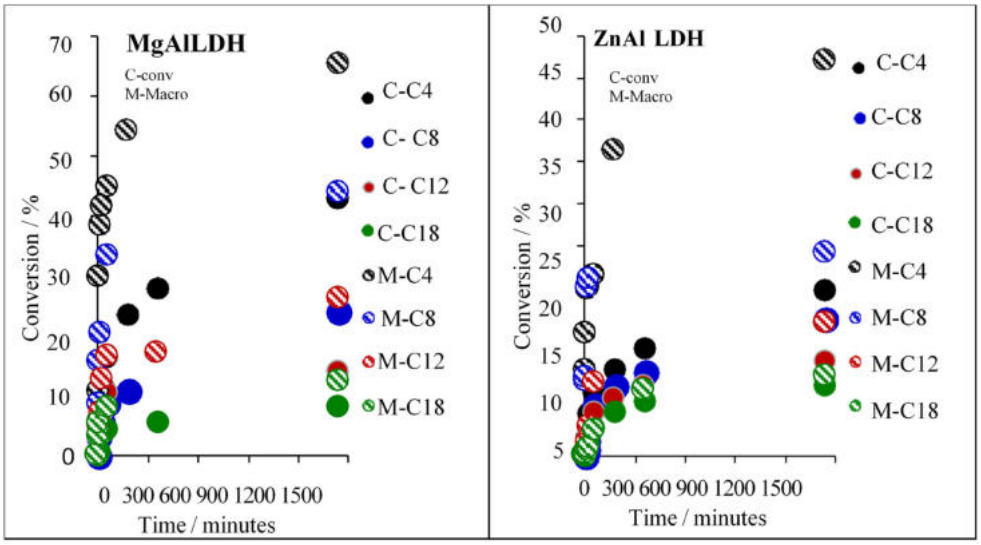

Fig. 8. Reaction profile illustrating C_4 C_{18} hydrocarbon production over standard and high-porosity MgAl-LDH (left) and ZnAl-LDH (right).

the ability to perform transesterification reactions in methanol under certain circumstances was measured over a period of 24 hours at a temperature of 110 °C and a speed of 650 rpm.[30] TAGs ranging from C4 to C18 were later analyzed to investigate the improvement in mass diffusion influenced by steric effects. Fig. 8 presents the conversion trends of various triglycerides during the reaction over the MgAlLDH and ZnAlLDH series. The graph illustrates that incorporating macroporosity significantly enhances conversion in all instances.

The observed enhancement in catalytic activity is attributed to improved mass transfer of bulkier TAG molecules, demonstrating that catalytic performance is increasingly influenced by pore accessibility as chain length grows. The addition of macropores in MacroMgAlLDH and MacroZnAlLDH systems significantly increased FAME production rates, improving conversion, yield, and turnover frequency (TOF). This effect becomes more pronounced with longer TAG chains due to aggravated diffusion limitations.[31] XRD analysis revealed that the LDH structure was retained post-modification, with a noticeable increase in lattice parameter a, suggesting enhanced interlayer spacing that may aid in substrate transport. SEM analysis confirmed the successful formation of macroporous frameworks, providing accessible channels for bulky molecules. BET analysis further supported this by showing an increased average pore diameter in MacroLDH catalysts, which facilitates the improved diffusion of the TAGs. Meanwhile, CO_2-TPD profiles indicated a reduction in both the number of active sites and basic sites density in both MacroLDHs, reinforcing that the observed catalytic improvements stem primarily from improved mass transport rather than increased surface reactivity.[11] This is substantiated by the formation profiles of key intermediates, dibutyrin and monobutyrin (Fig. 8), which peaked before being efficiently converted into FAME, evidencing both selectivity and reactivity. As shown in Fig. 9, the incorporation of macropores led to a dramatic rise in TOF—approximately 20-fold for MacroMgAlLDH and 15-fold for MacroZnAlLDH—relative to their conventional counterparts, underscoring the critical role of hierarchical porosity in overcoming diffusion barriers and enhancing catalytic efficiency in the transesterification of long-chain TAGs. Compared to the earlier work by Woodford et al.,[9] who

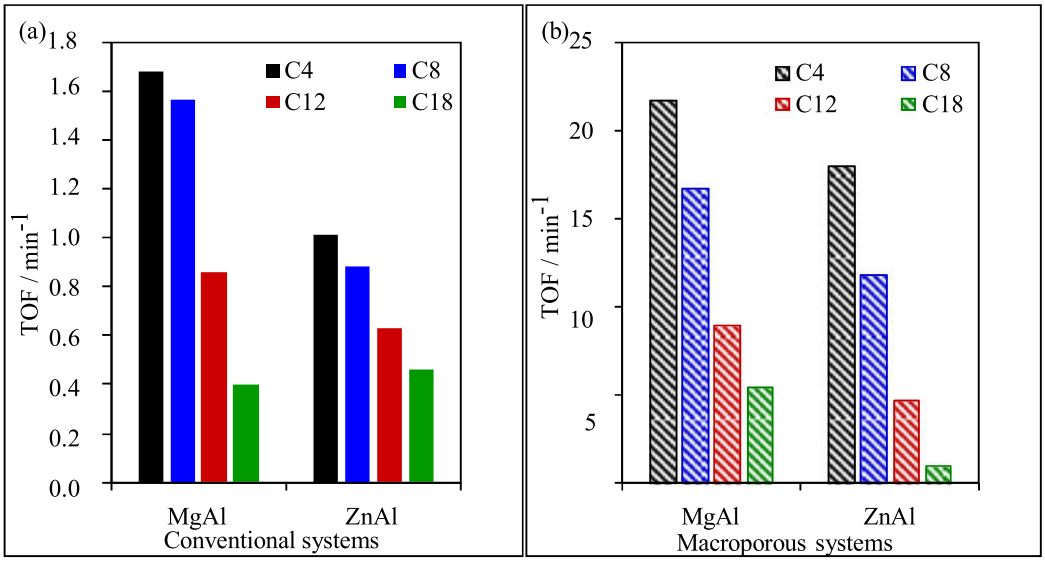

Fig. 9. Turnover frequency (TOF) trends for C4 – C18 production in standard and high-porosity MgAl-LDH (a) and ZnAl-LDH.

developed the first alkaline macroporous hydrotalcite using polystyrene (PS) beads and achieved up to a ~10-fold increase in turnover frequency (TOF) for the transesterification of C4–C18 esters, our optimized method demonstrates a significantly enhanced ability to convert triacylglycerols (TAGs) more efficiently and at a larger scale.

The use of macropores has significantly improved the catalytic efficiency of the transesterification reaction for model chain triglycerides spanning chain lengths from C4 to C18, possibly offering substantial advantages in the transesterification of actual oil feedstocks.[11,32] The TOFs of MgAl LDH are significantly greater than those of ZnAl LDH in both ConvHT and MacroHT conditions. The results indicate that the diffusion rate via the MgAlLDH series significantly exceeds that of the ZnAlLDH series. Both SEM and TEM demonstrated that the MacroMgAl had a larger pore size diameter than the MacroZnAlLDH. Larger pores provide increased diffusion, hence alleviating the constraints associated with diffusion in bulkier TAG.[33]

Conclusion

This study demonstrates that macroporous layered double hydroxides (LDHs) significantly enhance catalytic performance in biodiesel synthesis, achieving up to a 20-fold increase in turnover frequency (TOF), particularly with larger triglyceride molecules. This improvement is attributed to several key factors. Upon HTM reconstruction, crystallinity increased notably in both Mg- and Zn-based LDHs—rising to 85.3% in MacroMgAlLDH and to 70.5% in MacroZnAlLDH—indicating improved structural order and stability. The use of polystyrene (PS) templates introduced uniform macropores (106–146 nm), effectively increasing interparticle spacing and enhancing mass transport and active site accessibility. The observed increase in lattice parameters further supports the formation of larger crystallites. Although a slight reduction in basicity was noted—likely due to acidic residues from the PS templates—the catalytic performance remained high. This indicates that improved pore architecture and structural refinement, rather than basicity alone, play a dominant role in enhancing catalytic efficiency by effectively overcoming diffusion limitations commonly encountered in real-world biodiesel production. These results establish macroporous LDHs as a robust and scalable catalyst platform for advanced biodiesel production.

Acknowledgment

The author sincerely appreciates the valuable support provided by the Universiti Teknologi MARA (UiTM) Shah Alam and the Faculty of Applied Sciences. Special attribution goes to the Malaysia Ministry of Higher Education (MOHE) for funding this project under the grant of MyPair-STFC ISIS Muon Neutron Source, UK; 100-TNCPI/INT 16/6/2 (041/2024).

Authors declaration

- Conflicts of Interest: None.
- We hereby confirm that all the Figures and Tables in the manuscript are ours. Any Figures and images that are not ours have been included with

the necessary permission for re-publication, which is attached to the manuscript.
- No animal studies are present in the manuscript.
- No human studies are present in the manuscript.
- Ethical Clearance: The project was approved by the local ethical committee at Universiti Teknologi MARA, 40450 Shah Alam, Selangor, Malaysia.

Authors' contributions statement

NAT: Conducted the experiments, developed the main ideas and concepts, edited, wrote, and paraphrased the entire manuscript; created the figures and visualizations; supervised the research; and secured the funding.

MHH: Performed some experiments related to catalyst preparation and characterization.

NN: Contributed to editing and validating the data.

Data availability statement

The data supporting the findings of this study are available within the article.

Funding statements

Funding was received from the Malaysian Ministry of Higher Education (MOHE) under the grant number: MyPair-STFC ISIS Muon Neutron Source, UK; 100-TNCPI/INT 16/6/2 (041/2024).

References

1. Mohamed EA, Betiha MA, Negm NA. Insight into the Recent Advances in Sustainable Biodiesel Production by Catalytic Conversion of Vegetable Oils: Current Trends, Challenges, and Prospects. 2023;37:2631–47. https://doi.org/10.1021/acs.energyfuels.2c03887.
2. Hao T, Xu H, Sun S, Yu H, Qin Q, Song B, *et al.* Assembling flower-like MgAl-LDH nanospheres and g-C3N4 nanosheets for high efficiency removal of methyl orange. Ceram Int. 2024;50:10724–34. https://doi.org/10.1016/J.CERAMINT.2023.12.388.
3. Han H, Tang L, Wei K, Zhang S, Ma X, Ma C, *et al.* Restructuring surface frustrated Lewis pairs of MgAl-LDH through isomorphous Co doping for accelerating photocatalytic CO2 reduction. Sep Purif Technol. 2025;356:129800. https://doi.org/10.1016/J.SEPPUR.2024.129800.
4. Ahmad Tajuddin N, Manayil JC, Isaacs MA, Parlett CMA, Lee AF, Wilson K. Alkali-free zn–al layered double hydroxide catalysts for triglyceride transesterification. 2018;8:1–11. https://doi.org/10.3390/catal8120667.
5. Ahmad Tajuddin N, Manayil JC, Lee AF, Wilson K. Alkali-Free Hydrothermally Reconstructed NiAl Layered Double Hydroxides for Catalytic Transesterification. 2022;12:286–98. https://doi.org/10.3390/CATAL12030286/S1.
6. Huang Y, Liu C, Rad S, He H, Qin L. A Comprehensive Review of Layered Double Hydroxide-Based Carbon Composites as an Environmental Multifunctional Material for Wastewater Treatment. 2022;10:617. https://doi.org/10.3390/PR10040617.
7. Li D, Chen M, Jiang Y. Adsorptive removal of phosphate by ZnAlLa ternary layered double hydroxides: Synthesis conditions, adsorption performance, mechanism and reusability. Sep Purif Technol. 2025;354:128668. https://doi.org/10.1016/j.seppur.2024.128668.
8. Géraud E, Prévot V, Leroux F. Synthesis and characterization of macroporous MgAl LDH using polystyrene spheres as template. J Phys Chem Solids. 2006;67:903–8. https://doi.org/10.1016/j.jpcs.2006.01.002.
9. Woodford JJ, Dacquin JP, Wilson K, Lee AF. Better by design: nanoengineered macroporous hydrotalcites for enhanced catalytic biodiesel production. Energy Environ Sci. 2012;5:6145. https://doi.org/10.1039/c2ee02837a.
10. Ioan-Cezar M, Pavel OD. Layered Double Hydroxide-Based Catalytic Materials for Sustainable Processes. 2022. https://doi.org/10.3390/books978-3-0365-4980-4.
11. Ahmad Tajuddin N. Novel Alkali-Free of Layered Double Hydroxide and Solid Base Catalysts For Transesterification of C4-C18 Triglycerides. 2017.
12. Rabee AIM, Manayil JC, Isaacs MA, Parlett CMA, Durndell LJ, Zaki MI, *et al.* On the Impact of the Preparation Method on the Surface Basicity of Mg–Zr Mixed Oxide Catalysts for Tributyrin Transesterification. Catal 2018, Vol 8, Page 228. 2018;8:228. https://doi.org/10.3390/CATAL8060228.
13. Zhang X, Yang S, Xie X, Chen L, Sun L, Zhao B, *et al.* Stoichiometric synthesis of Fe/CaxO catalysts from tailored layered double hydroxide precursors for syngas production and tar removal in biomass gasification. J Anal Appl Pyrolysis. 2016;120:371–8. https://doi.org/10.1016/j.jaap.2016.06.005.
14. Bernardo MP, Moreira FKV, Colnago LA, Ribeiro C. Physicochemical assessment of [Mg-Al-PO4]-LDHs obtained by structural reconstruction in high concentration of phosphate. Colloids Surf, A. 2016;497:53–62. https://doi.org/10.1016/j.colsurfa.2016.02.021.
15. Baoyu C, Jiehu C, Chang L, Jiamin F, Shuxia W, Xiuhong D, *et al.* Synthesis of MgAl-LDH from three alkali sources for boosting flame retardancy of EP with APP. 2024;447:137997. https://doi.org/10.1016/J.CONBUILDMAT.2024.137997.
16. Sun M, Wang XZ, Xiong RY, Chen X, Zhai LF, Wang S. High-performance biochar-loaded MgAl-layered double oxide adsorbents derived from sewage sludge towards nanoplastics removal: Mechanism elucidation and QSAR modeling. Sci Total Environ. 2023;901:165971. https://doi.org/10.1016/J.SCITOTENV.2023.165971.
17. Kamal NA, Pungot NH, Che Soh SK, Ahmad Tajuddin N. Facile and green hydrothermal synthesis of MgAl/NiAl/ZnAl layered double hydroxide nanosheets: a physiochemical comparison. Pure Appl Chem. 2024;96:1667–82. https://doi.org/10.1515/pac-2024-0014.
18. Szabó V, Mészáros R, Kutus B, Samu GF, Kónya Z, Kukovecz á, *et al.* Sonochemically improved regeneration of mechanically amorphized Ca2Cr-layered double hydroxides — Synthesis, characterization and photocatalytic lidocaine decomposition. Appl Clay Sci. 2025;265:107684. https://doi.org/10.1016/J.CLAY.2024.107684.
19. Thommes M, Kaneko K, Neimark A V., Olivier JP, Rodriguez-Reinoso F, Rouquerol J, et al. Physisorption of gases, with special reference to the evaluation of surface area and pore size distribution (IUPAC Technical Report). Pure Appl Chem. 2015;87:1051–69. https://doi.org/10.1515/PAC-2014-1117.

20. Zhang Y, Yong C, Yan Z, Luo S, Jing F, Chu W. Influence of hydrothermal treatment on structural property of NiZrAl mixed-metal oxides and on catalytic steam reforming of glycerol for hydrogen production. Int J Hydrog Energy. 2020;45:22448–58. https://doi.org/10.1016/J.IJHYDENE.2020.06.104.
21. Jung JS, Hong GH, Park JI, Yang EH, Hodala JL, Moon DJ. Effect of Cobalt Supported on Meso-Macro Porous Hydrotalcite in Fischer-Tropsch Synthesis. RSC Adv. 2016;6:104280–93. https://doi.org/10.1039/C6RA17206G.
22. Li C, Wang L, Wei M, Evans DG, Duan X. Large oriented mesoporous self-supporting Ni–Al oxide films derived from layered double hydroxide precursors. J Mater Chem. 2008;18:2666–72. https://doi.org/10.1039/B801620H.
23. Woodford JJ, Dacquin JP, Wilson K, Lee AF. Better by design: nanoengineered macroporous hydrotalcites for enhanced catalytic biodiesel production. Energy Environ Sci. 2012;5:6145. https://doi.org/10.1039/c2ee02837a.
24. Mustapha AO, Rasaq SO, Raimi MT, Amisu SK, Bello FP, Afolabi YT, *et al.* Synthesis, Characterization and Properties of Trimethylolpropane Triesters from Coconut (Cocos nucifera) Methyl Esters. Baghdad Sci J. 2023;20:2478–2478. https://doi.org/10.21123/BSJ.2023.8384.
25. Alwash A. The Green Synthesize of Zinc Oxide Catalyst Using Pomegranate Peels Extract for the Photocatalytic Degradation of Methylene Blue Dye. Baghdad Sci J. 2020;17:0787–0787. https://doi.org/10.21123/BSJ.2020.17.3.0787.
26. Praveen BVS, Pradhan NC, Ashok A, Guduru RK, Vij RK, Jeeru LR. Production of biodiesel: kinetics and reusability studies of the Mg–Al hydrotalcite catalyst using Jatropha oil. React Chem Eng. 2023; https://doi.org/10.1039/D2RE00543C.
27. Yang C, Wang L, Yu Y, Wu P, Wang F, Liu S, *et al.* Highly efficient removal of amoxicillin from water by Mg-Al layered double hydroxide/cellulose nanocomposite beads synthesized through in-situ coprecipitation method. Int J Biol Macromol. 2020;149:93–100. https://doi.org/10.1016/j.ijbiomac.2020.01.096.
28. Montanari T, Sisani M, Nocchetti M, Vivani R, Concepcion Herrera Delgado M, Ramis G, *et al.* Zinc-aluminum hydrotalcites as precursors of basic catalysts: Preparation, characterization and study of the activation of methanol. Catal Today. 2010;152:104–9. https://doi.org/10.1016/j.cattod.2009.09.012.
29. Naumkin AV, Kraut-Vass A, Gaarenstroom SW, Cedric JP. NIST Standard Reference Database 20, Version 4.1. [Internet]. 2012.
30. Pei San K. A Novel Hydrophobic ZrO2-SiO2 Based Heterogeneous Acid Catalyst for the Esterification of Glycerol with Oleic Acid. 2018.
31. Villarruel EMO, de Carvalho Filho JFS, Garcia MAS, de Almeida JMAR, Aranda DAG, Romano PN. Maintaining high-triglyceride content and reducing free fatty acids in distillers corn oil: A catalyst-free multivariate strategy. J Am Oil Chem Soc. 2024;101:575–87. https://doi.org/10.1002/AOCS.12802.
32. Hamzah N, Yusof I, Zurina Samad W, Hanim Saleh S, Ahmad Tajuddin N, Lokman Ibrahim M. Production of Biodiesel From Waste Cooking Oil Using Bentonite Catalysts. Vol. 9, Journal of Academia. 2021. p. 139–144.
33. Yusuf BO, Oladepo SA, Ganiyu SA, Peedikakkal AMP. Synthesis and evaluation of CuO/UiO-66 metal-organic frameworks as a solid catalyst for biodiesel production from waste cooking oil. Mol Catal. 2024;564:114313. https://doi.org/10.1016/J.MCAT.2024.114313.

التصميم البنيوي للمحفزات ذات الطبقات المزدوجة الواسعة المسامية: تخفيف قيود نقل الكتلة في ثلاثي الغليسريدات الأكبر حجمًا

نزرزواتي أحمد تاج الدين[1]، محمد هداية حيدر[2]، نزار الدين نزار الدين[2]

[1] كلية الكيمياء والبيئة، كلية العلوم التطبيقية، جامعة مارا للتكنولوجيا، 40450 شاه علم، سيلانغور، ماليزيا.
[2] قسم الهندسة الكيميائية، كلية العلوم والتكنولوجيا، جامعة جامبي، 36361، جامبي، إندونيسيا.

الملخص

تُعدّ الهيدروكسيدات المزدوجة الطبقات (LDHs) محفزاتٍ واعدة لإنتاج الوقود الحيوي (الديزل الحيوي) من خلال عملية الأسترة التحويلية للغليسريدات الثلاثية(TAGs) ، غير أنّ قيود انتقال الكتلة تحدّ من فعاليتها، خصوصاً مع جزيئات الغليسريدات الثلاثية الأكبر حجماً. تتناول هذه الدراسة هذه المشكلة من خلال تحضير مواد ماكرو-مسامية من MgAl-LDH و ZnAl-LDHباستخدام طريقة القالب المصنوع من البوليسترين. أظهرت عمليات التحليل الشاملة تكوينَ بنى ماكرو-مسامية ناجحة تمتاز بتحسّن ملحوظ في الخصائص الفيزيائية والكيميائية والبنية التركيبية مقارنة بالـ LDHs التقليدية. وقد أكّد حيود الأشعة السينية (XRD) إعادة تكوين بنية الـ LDH بنجاح بعد عمليتي التكليس وإعادة الترطيب، مع ملاحظة زيادة في درجة التبلور في المواد الماكرو-مسامية. كما أظهر تحليل مساحة السطح بطريقة BET زيادة كبيرة) بحوالي عشرة أضعاف في حالة (MgAl-LDH في الإطار الماكرو-مسامي. وكشفت صور المجهر الإلكتروني الماسح (SEM) والمجهر الإلكتروني النافذ (TEM) عن شبكة مسامية واسعة بمتوسط قطر للمسام يقارب 300 نانومتر، بما يتوافق مع أبعاد قالب البوليسترين المستخدم. أما تحليل الطيف الإلكتروني للأشعة السينية (XPS) فقد أظهر تغيرات طفيفة في التركيب العنصري السطحي وحالات الأكسدة، مما يشير إلى تأثير البنية الماكرو-مسامية على الخصائص السطحية. أظهرت الاختبارات التحفيزية باستخدام غليسريدات ثلاثية مختلفة) من C4 إلى (C18 تحسناً ملحوظاً في النشاط التحفيزي، خصوصاً للغليسريدات الأعلى وزناً جزيئياً، نتيجة لتحسن انتقال الكتلة. كما تجاوزت الترددات الدورانية للمحفزات الماكرو-مسامية نظيراتها في الـ LDHs التقليدية بما يقارب عشرين ضعفاً في نظام MgAl-LDH وخمسة عشر ضعفاً في نظام ZnAl-LDH. تؤكد هذه النتائج كفاءة الهيدروكسيدات المزدوجة الطبقات الماكرو-مسامية كمحفزات فعالة جداً لإنتاج الديزل الحيوي، لقدرتها على تجاوز القيود الجوهرية في انتقال الكتلة التي تعاني منها المحفزات التقليدية.

الكلمات المفتاحية: الديزل الحيوي، الهيدروكسيدات المزدوجة الطبقات ((LDH، المسامية الكبيرة (الماكرو-مسامية)، انتقال الكتلة، الغليسريدات الثلاثية.